Electronic Supplemental Information

Folding of an opened spherical shell

E. Couturier[1*], J. Dumais[2], E. Cerda[1], E. Katifori[3]

[1] Departamento de Física, Universidad de Santiago de Chile, Santiago, Chile
[2] Faculdad de Ingeniería y Ciencias, Universidad Adolfo Ibáñez, Viña del Mar, Chile
[3] Max Planck Institute for Dynamics and Self-Organization (MPIDS), Goettingen, Germany
*To whom correspondence should be addressed; E-mail: couturier.etienne@yahoo.fr.

1 Derivation of the fundamental forms of a surface with an n-fold symmetry of rotation.

1.1 Fundamental forms of a constant Gaussian curvature surfaces

For completeness, here we provide a detailed derivation of the fundamental forms of a constant Gaussian curvature surface (Spivak, 1979).

The first and second fundamental forms of a surface $S(u,v)$ read:

$$I = Edu^2 + 2Fdudv + Gdv^2 \quad (12)$$
$$II = Ldu^2 + 2Mdudv + Ndv^2 \quad (13)$$

We perform a change of coordinates, so that $z = u+iv$ and $\bar{z} = u-iv$. In this coordinate system the fundamental forms become:

$$I = E'dz^2 + 2F'dzd\bar{z} + G'd\bar{z}^2$$
$$II = L'dz^2 + 2M'dzd\bar{z} + N'd\bar{z}^2$$

where

$$E' = (E - G + 2F/i)/4$$
$$F' = (E + G)/2$$
$$G' = (E - G - 2F/i)/4$$
$$L' = (L - N + 2M/i)/4$$
$$M' = (L + N)/2$$
$$N' = (L - N - 2M/i)/4$$

These equations can be simplified further in the case of a constant Gaussian curvature surface of positive curvature K. Klotz (Klotz, 1963) defines:

$$\hat{\Omega} = ((E-G)/2 - iF)(du + idv)^2 \tag{14}$$

for $L = N = \mu$, and $M = 0$ and shows that iff $K = const > 0$, then the function $\hat{\Omega}$ is a holomorphic quadratic differential. This is equivalent to $L' = N' = 0$ and $E' = \frac{\phi}{K}$ where ϕ is an holomorphic function of z ($G' = \frac{\bar{\phi}}{K}$ is automatically antiholomorphic). It has been proved that the first and second fundamental forms, expressed in this form, verify automatically the two Codazzi equations (Klotz, 1963).

As F' is a positive real number, without loss of generality we can express it as the following expression of an undetermined function ω and of $|\phi|$.

$$F' = \frac{e^{2\omega} + |\phi|^2 e^{-2\omega}}{2K} \tag{15}$$

ω and ϕ are linked by the Gauss equation for a surface with constant Gaussian curvature. The Liouville writing of the Gauss equation reads:

$$K = -\frac{1}{2\sqrt{E'G' - F'^2}} \left(\frac{\partial}{\partial z}\left(\frac{G'_z + F'G'_{\bar{z}}/G' - 2F'_{\bar{z}}}{\sqrt{E'G' - F'^2}}\right) + \frac{\partial}{\partial \bar{z}}\left(\frac{E'_{\bar{z}} - F'G'_z/G'}{\sqrt{E'G' - F'^2}}\right) \right)$$

As E' is holomorphic (i.e $E'_{\bar{z}} = 0$), and G' is antiholomorphic (i.e $G'_z = 0$), it simplifies to:

$$K = -\frac{1}{2\sqrt{E'G' - F'^2}} \frac{\partial}{\partial z}\left(\frac{F'G'_{\bar{z}} - 2G'F'_{\bar{z}}}{G'\sqrt{E'G' - F'^2}}\right) \tag{16}$$

Using the intermediate result:

$$(E'G' - F'^2)K^2 = |\phi|^2 - \left(\frac{e^{2\omega} + |\phi|^2 e^{-2\omega}}{2}\right)^2 = -\left(\frac{e^{2\omega} - |\phi|^2 e^{-2\omega}}{2}\right)^2 \tag{17}$$

after some algebra the expression (16) reads:

$$K = \frac{-4K\omega_{z\bar{z}}}{e^{2\omega} - |\phi|^2 e^{-2\omega}} \tag{18}$$

As $\triangle\omega = 4\omega_{z\bar{z}}$, we finally obtain a variant of the sinh-Gordon equation linking ω and ϕ:

$$\triangle\omega + (e^{2\omega} - |\phi|^2 e^{-2\omega}) = 0 \tag{19}$$

As $K = \frac{-M'^2}{E'G' - F'^2}$, using (17) we get:

$$M' = \frac{e^{2\omega} - |\phi|^2 e^{-2\omega}}{2\sqrt{K}}$$

1.1.1 Fundamental forms of constant Gaussian curvature surfaces with a symmetry of rotation of order n

We now derive the fundamental forms for a surface with symmetry of rotation. We first perform a change of coordinates from $(z, \overline{z})$ to polar coordinates (ρ, θ), where $z = \rho e^{i\theta}$. By simple substitution in the expressions for the first and second fundamental form and after some algebra, we get:

$$\begin{aligned} I &= \frac{\phi e^{2i\theta}(d\rho + i\rho d\theta)^2 + (e^{2\omega} + |\phi|^2 e^{-2\omega})(d\rho^2 + \rho^2 d\theta^2) + \bar{\phi} e^{-2i\theta}(d\rho - i\rho d\theta)^2}{K} \\ II &= \frac{(e^{2\omega} - |\phi|^2 e^{-2\omega})(d\rho^2 + \rho^2 d\theta^2}{\sqrt{K}} \end{aligned} \tag{20}$$

The three coefficients $\tilde{E}$, $\tilde{F}$ and $\tilde{G}$ of the first fundamental form, and the three coefficients $\tilde{L}$, $\tilde{M}$ and $\tilde{N}$ of the second fundamental form expressed in polar coordinates read:

$$\begin{aligned} \tilde{E} &= \frac{2Re(\phi e^{2i\theta}) + e^{2\omega} + |\phi|^2 e^{-2\omega}}{K} \\ \tilde{F} &= \frac{-2\rho Im(\phi e^{2i\theta})}{K} \\ \tilde{G} &= \frac{\rho^2(-2Re(\phi e^{2i\theta}) + e^{2\omega} + |\phi|^2 e^{-2\omega})}{K} \\ \tilde{L} &= \frac{(e^{2\omega} - |\phi|^2 e^{-2\omega})}{\sqrt{K}} \\ \tilde{M} &= 0 \\ \tilde{N} &= \frac{\rho^2(e^{2\omega} - |\phi|^2 e^{-2\omega})}{\sqrt{K}} \end{aligned} \tag{21}$$

The fundamental forms of an n-fold rotationally symmetric surface have to be n-fold rotationally symmetric in θ. Thus, if I and II have a rotational symmetry of order n then:

$$\omega(r, \theta) = \Omega(r, n\theta) \tag{22}$$

for some function Ω, and ϕ equals:

$$\phi = z^{-2} \sum_{k=1}^{\infty} \alpha_k z^{kn} \tag{23}$$

To derive the fundamental form presented in the article, we used the special case $\phi = -\lambda z^{n-2}$ where λ is a parameter independant of z.

1.1.2 Derivation of the Bonnet ODE system determining the surface.

For completeness, here we derive the system of ODEs that determine the surface. The basic theory is detailed in all basic textbooks of differential geometry (Spivak, 1979). In particular, we outline some intermediate results of the algebraic calculations that pertain to our system of ODEs. To simplify the calculations that follow, we introduce the notation below:

$$\begin{aligned} A &= \frac{Re(\phi e^{2i\theta})}{K} \\ B &= \frac{Im(\phi e^{2i\theta})}{K} \\ C &= \frac{e^{2\omega}+|\phi|^2 e^{-2\omega}}{K} \\ S &= \frac{e^{2\omega}-|\phi|^2 e^{-2\omega}}{K} \end{aligned} \tag{24}$$

The two fundamental forms now read:

$$\begin{aligned} \tilde{E} &= 2A + C \\ \tilde{F} &= -2\rho B \\ \tilde{G} &= \rho^2(-2A + C) \\ \tilde{L} &= \sqrt{K}S \\ \tilde{M} &= 0 \\ \tilde{N} &= \rho^2\sqrt{K}S \end{aligned} \tag{25}$$

To calculate the Christoffel symbols, we need to evaluate the following derivatives:

$$\begin{aligned} \tilde{E}_\rho &= 2A_\rho + 2\omega_\rho S + 2Re(\phi\overline{\phi_\rho})e^{-2\omega} \\ \tilde{E}_\theta &= 2A_\theta + 2\omega_\theta S + 2Re(\phi\overline{\phi_\theta})e^{-2\omega} \\ \tilde{F}_\rho &= -2(B + \rho B_\rho) \\ \tilde{F}_\theta &= -2\rho B_\theta \\ \tilde{G}_\rho &= \rho^2(-2A_\rho + 2\omega_\rho S + 2Re(\phi\overline{\phi_\rho})e^{-2\omega}) + 2\rho(-2A + C) \\ \tilde{G}_\theta &= \rho^2(-2A_\theta + 2\omega_\theta S + 2Re(\phi\overline{\phi_\theta})e^{-2\omega}) \end{aligned} \tag{26}$$

For $\phi = -\lambda z^{n-2}$ we get:

$$\begin{aligned} A &= \frac{-\lambda\rho^{n-2}\cos(n\theta)}{K} \\ B &= -\frac{\lambda\rho^{n-2}\sin(n\theta)}{K} \\ A_\rho &= -\frac{(n-2)\lambda\rho^{n-3}\cos(n\theta)}{K} \\ A_\theta &= \frac{n\lambda\rho^{n-2}\sin(n\theta)}{K} \\ B_\rho &= -\frac{(n-2)\lambda\rho^{n-3}\sin(n\theta)}{K} \\ B_\theta &= -\frac{n\lambda\rho^{n-2}\cos(n\theta)}{K} \end{aligned} \tag{27}$$

Finally, the Christoffel symbols read:

$$\begin{aligned} \Gamma^1_{11} &= \frac{\tilde{G}\tilde{E}_\rho - \tilde{F}(2\tilde{F}_\rho - \tilde{E}_\theta)}{2(\tilde{E}\tilde{G} - \tilde{F}^2)} \\ \Gamma^2_{11} &= \frac{-\tilde{F}\tilde{E}_\rho + \tilde{E}(2\tilde{F}_\rho - \tilde{E}_\theta)}{2(\tilde{E}\tilde{G} - \tilde{F}^2)} \\ \Gamma^1_{12} &= \frac{\tilde{G}\tilde{E}_\theta - \tilde{F}\tilde{G}_\rho}{2(\tilde{E}\tilde{G} - \tilde{E}^2)} \\ \Gamma^2_{12} &= \frac{-\tilde{F}\tilde{E}_\theta + \tilde{E}\tilde{G}_\rho}{2(\tilde{E}\tilde{G} - \tilde{F}^2)} \\ \Gamma^1_{22} &= \frac{\tilde{G}(2\tilde{F}_\theta - \tilde{G}_\rho) - \tilde{F}\tilde{G}_\theta}{2(\tilde{E}\tilde{G} - \tilde{F}^2)} \\ \Gamma^2_{22} &= \frac{-\tilde{F}(2\tilde{F}_\theta - \tilde{G}_\rho) + \tilde{E}\tilde{G}_\theta}{2(\tilde{E}\tilde{G} - \tilde{F}^2)} \end{aligned} \tag{28}$$

and the ODE system that determines the surface S and its normal $\mathcal{N}$ is found to be:

$$S_{\rho\rho} = \Gamma^1_{11}S_\rho + \Gamma^2_{11}S_\theta + \tilde{L}\mathcal{N} \tag{29}$$

$$S_{\rho\theta} = \Gamma^1_{12}S_\rho + \Gamma^2_{12}S_\theta \tag{30}$$

$$S_{\theta\theta} = \Gamma^1_{22}S_\rho + \Gamma^2_{22}S_\theta + \tilde{N}\mathcal{N} \tag{31}$$

$$\mathcal{N}_\rho = \frac{\tilde{L}(-\tilde{G}S_\rho + \tilde{F}S_\theta)}{\tilde{E}\tilde{G} - \tilde{F}^2} \tag{32}$$

$$\mathcal{N}_\theta = \frac{\tilde{N}(\tilde{F}S_\rho - \tilde{E}S_\theta)}{\tilde{E}\tilde{G} - \tilde{F}^2} \tag{33}$$

The different equations of the ODE system should be compatible following the Gauss-Codazzi equations. In our case, as the Gauss equation is only solved to zeroth order in λ, the different equations of the ODE system we get using our approximate ω solution are not compatible anymore. To get our family of approximately constant Gaussian curvature surfaces we integrated the system constituted by the equations corresponding to the ρ derivative (29, 30, 32) along the ρ coordinate with the following set of initial conditions:

$$\begin{aligned} S(\rho_0,\theta) &= [0,0,0] \\ S_\rho(\rho_0,\theta) &= \sqrt{\tilde{E}}[\cos(\theta),\sin(\theta),0] \\ S_\theta(\rho_0,\theta) &= \frac{\tilde{F}}{\sqrt{\tilde{E}}}[\cos(\theta),\sin(\theta),0] + \frac{\sqrt{\tilde{E}\tilde{G}-\tilde{F}^2}}{\sqrt{\tilde{E}}}[-\sin(\theta),\cos(\theta),0] \end{aligned} \tag{34}$$

where $\tilde{E},\tilde{F},\tilde{G}$ are calculated at (ρ_0,θ).

Even if the surface is perfectly defined in $\rho = 0$, the angular coordinate makes the coefficient of the ODE artificially divergent at 0. The initial conditions correspond to a very small but strictly positive ρ_0. The value of ρ_0 depends of the function ω. The bigger the $\omega(0,\theta)$ value is, the smaller is ρ_0. This procedure is described in detail for the dual problem of constant mean curvature surfaces in (Dos Reis, 2003).

If the full sinh-Gordon equation was solved, then the integration along ρ and along θ would commute. Now, as the pseudo-fundamental forms do not fullfil the Gauss equation exactly, this is not true anymore. Nevertheless the surface we get by integrating the Pseudo-Bonnet system along ρ is smooth and well defined. A way to prove it is to see the peudo-Bonnet system as an ODE system in ρ whose coefficients depend of ρ and on a θ. As we removed the singularities of our integration domain, these coefficients are C^∞ in both ρ and θ. As such, the flow (the quasi CGC surface) is both C^∞ in the variable ρ and the parameter θ (Berger, 1992). We can notice that except for the term E the pseudo-fundamental forms do correspond to the real fundamental forms of the surface.

1.2 Analytic calculation of the line in the planes of symmetry

In this section we outline the analytic calculation of the trajectory of the cross section at one of the n planes of symmetry of our n-fold symmetric structure. As presented in the main text, the family of quasi-CGC surfaces was obtained using $\phi = -\lambda z^{n-2}$ and $\omega = \log \frac{2\mu|(1+(n-1)z^n)|}{|(1-z^n)|^2+\mu^2|z|^2}$. At fixed ρ, the function ω reaches its extremum ($\omega_\theta = 0$) when z is real for $\theta = \frac{k\pi}{n}$. For these angles, the coefficient of the fundamental forms and their

derivatives simplify considerably:

$$\begin{aligned}
\tilde{E}(\rho, \frac{k\pi}{n}) &= \frac{-2\lambda\rho^{n-2}(-1)^k}{K} + C(\rho, \frac{k\pi}{n}) = \frac{(e^{\omega} - (-1)^k\lambda\rho^{n-2}e^{-\omega})^2}{K} \\
\tilde{E}_{\theta}(\rho, \frac{k\pi}{n}) &= 0 \\
\tilde{F}(\rho, \frac{k\pi}{n}) &= 0 \\
\tilde{G}(\rho, \frac{k\pi}{n}) &= \frac{\rho^2(2(-1)^k\lambda\rho^{n-2})}{K} + C(\rho, \frac{k\pi}{n}) = \frac{\rho^2(e^{\omega} + (-1)^k\lambda\rho^{n-2}e^{-\omega})^2}{K}
\end{aligned} \tag{35}$$

One of the Christoffel symbol is also zero $\Gamma^2_{11} = 0$. So the ODE system simply reads :

$$\begin{aligned}
S_{\rho\rho} &= \Gamma^1_{11}S_{\rho} + \tilde{L}\mathcal{N} \\
\mathcal{N}_{\rho} &= \frac{-\tilde{L}S_{\rho}}{\tilde{E}}
\end{aligned} \tag{36}$$

The line that we get by integrating along the ρ coordinate remains in the plane ($\mathcal{N}(0, \frac{2k\pi}{n})$, $S_{\rho}(0, \frac{2k\pi}{n})$) . These planes are the planes of symmetry of the surface.

As the solution remains in the plane, after a rotation by angle $-\frac{k\pi}{n}$ around the central axis of the surface, $\mathcal{N}$ and S_{ρ} read:

$$\begin{aligned}
\mathcal{N} &= [x(\rho), 0, -\sqrt{1 - x(\rho)^2}] \\
S_{\rho} &= \sqrt{\tilde{E}}[\sqrt{1 - x(\rho)^2}, 0, x(\rho)]
\end{aligned} \tag{37}$$

for some x,y function of ρ. So the ODE for the normal gives

$$x_{\rho} = \frac{-\tilde{L}\sqrt{1 - x(\rho)^2}}{\sqrt{\tilde{E}}} \tag{38}$$

The Gaussian curvature is:

$$K = \frac{\tilde{L}\tilde{N}}{\tilde{E}\tilde{G}} = \frac{\rho^2\tilde{L}^2}{\tilde{E}\tilde{G}} \tag{39}$$

from which we can easily derive:

$$\frac{\tilde{L}}{\sqrt{\tilde{E}}} = (e^{\omega} + (-1)^k\lambda\rho^{n-2}e^{-\omega}) \tag{40}$$

Eventually, the ODE for x reads:

$$x_{\rho} = -(e^{\omega} - (-1)^k\lambda\rho^{n-2}e^{-\omega})\sqrt{1 - x(\rho)^2} \tag{41}$$

As at $x(\rho = 0) = 0$ the normal is facing vertically downwards, the solution is simply found to be:

$$x = \sin(\int_0^\rho (e^\omega - (-1)^k \lambda \rho^{n-2} e^{-\omega})) \tag{42}$$

Then S_ρ reads:

$$\begin{aligned} S_\rho &= \sqrt{\tilde{E}}[\sqrt{1 - x(\rho)^2}, 0, x(\rho)] \\ S_\rho &= \frac{(e^\omega - (-1)^k \lambda \rho^{n-2} e^{-\omega})}{\sqrt{K}} \\ & \quad [\cos(\int_0^\rho (e^\omega + (-1)^k \lambda \rho^{n-2} e^{-\omega})), 0, \sin(\int_0^\rho (e^\omega + (-1)^k \lambda \rho^{n-2} e^{-\omega}))] \end{aligned}$$

and S reads:

$$S = \int_0^\rho \frac{(e^\omega - (-1)^k \lambda \rho^{n-2} e^{-\omega})}{\sqrt{K}} [\cos(\int_0^\rho (e^\omega + (-1)^k \lambda \rho^{n-2} e^{-\omega})), 0, \sin(\int_0^\rho (e^\omega + (-1)^k \lambda \rho^{n-2} e^{-\omega}))] \tag{43}$$

For k odd, these lines correspond to the lines that go through the singularity and for k even, they correspond to the lines that reach the top of the shell.

1.3 Analytical prediction for the line situated in the symmetry plane of the sphere

The integrals of the previous paragraph can be calculated analytically. We illustrate the integration for symmetry $n = 3$.

The solution for the line segment that reaches the top of the shell ($\theta = 0$) reads:

$$\begin{aligned} x &= \int_0 \frac{(e^\omega - \lambda \rho e^{-\omega})}{\sqrt{K}} \cos(\int_0 (e^\omega + \lambda \rho e^{-\omega})) \\ y &= 0 \\ z &= \int_0 \frac{(e^\omega - \lambda \rho e^{-\omega})}{\sqrt{K}} \sin(\int_0 (e^\omega + \lambda \rho e^{-\omega})) \end{aligned} \tag{44}$$

where ω evaluated at $(\rho, \theta = 0)$ reads :

$$\omega = \log \frac{2\mu(1 + 2\rho^3)}{(1 - \rho^3)^2 + \mu^2 \rho^2} \tag{45}$$

The integral in the cos and sin reads:

$$\begin{aligned}\int (e^{\omega}-\lambda\rho e^{-\omega}) &= 2\arctan(\frac{\mu\rho}{1-\rho^3})\chi_{\rho\leqslant 1}+2(\pi+\arctan(\frac{\mu\rho}{1-\rho^3}))\chi_{\rho>1}\\ &+ \frac{\lambda}{2\mu}\Big[-(\frac{\rho^5}{10}-\frac{5\rho^2}{8}+\frac{\mu^2\rho}{2})\\ &+ \frac{1}{24\ 2^{2/3}}(\left(2^{4/3}\mu^2+9\right)\left(2\log\left(2^{1/3}\rho+1\right)-\log\left(2^{2/3}\rho^2-2^{1/3}\rho+1\right)\right)+\\ &\quad 2\sqrt{3}\left(2^{4/3}\mu^2-9\right)(\arctan\left(\frac{2^{4/3}\rho-1}{\sqrt{3}}\right)+\arctan\left(\frac{1}{\sqrt{3}}\right)))\Big] \qquad (46)\end{aligned}$$

The solution for the line segment that passes through the singularity ($\theta=\pi$) reads:

$$\begin{aligned}x &= -\int_0 \frac{(e^{\omega}+\lambda\rho e^{-\omega})}{\sqrt{K}}\cos(\int_0(e^{\omega}-\lambda\rho e^{-\omega}))\\ y &= 0\\ z &= \int_0 \frac{(e^{\omega}+\lambda\rho e^{-\omega})}{\sqrt{K}}\sin(\int_0(e^{\omega}-\lambda\rho e^{-\omega})) \qquad (47)\end{aligned}$$

where ω evaluated at $(\rho,\theta=\pi)$ reads :

$$\omega=\log\frac{2\mu(1-2\rho^3)}{(1+\rho^3)^2+\mu^2\rho^2} \qquad (48)$$

The integral in the cos and sin reads:

$$\begin{aligned}&\int (e^{\omega}+\lambda\rho e^{-\omega}) = 2\arctan(\frac{\mu\rho}{1+\rho^3})+\frac{\lambda}{2\mu}\Big[-(\frac{\rho^5}{10}+\frac{5\rho^2}{8}+\frac{\mu^2\rho}{2})+\\ &+\frac{1}{24\ 2^{2/3}}(\left(2^{4/3}\mu^2+9\right)\left(-2\log\left(-2^{1/3}\rho+1\right)+\log\left(2^{2/3}\rho^2+2^{1/3}\rho+1\right)\right)+\\ &2\sqrt{3}\left(2^{4/3}\mu^2-9\right)(\arctan\left(\frac{2^{4/3}\rho+1}{\sqrt{3}}\right)-\arctan\left(\frac{1}{\sqrt{3}}\right)))\Big] \qquad (49)\end{aligned}$$

For very high μ, small ρ and λ, parameters which correspond to the small deformation of the sphere, these equations can even be fully integrated.

2 Computation of Gaussian curvature

The Gaussian curvature was computed using three independent methods: by a rough numerical differentiation scheme, by fitting splines and by calculating the derivatives or by the angle deficit method. All three methods give statistically indistinguishable results. The 5% threshold corresponds to the variation range observed for the experimental deformation of the ping-pong ball (see main text section 3.1).

The gaussian curvature of the approximate CGC solution oscillates around a constant equal to the gaussian curvature of the undeformed sphere. The amplitude of the oscillation increases with the geodesic distance to the umbilic (See Figure 1).

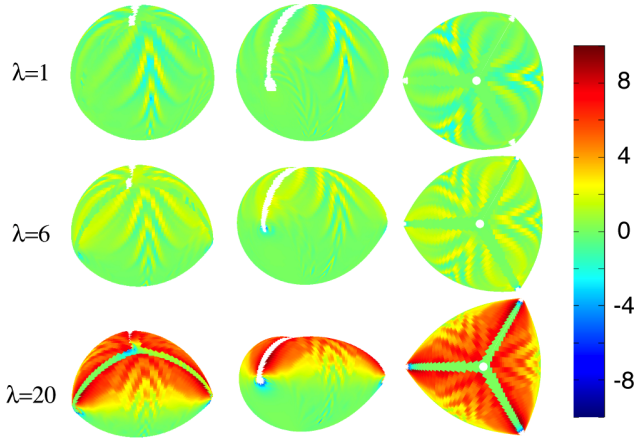

Figure 1: Gaussian curvature of the QCGC surfaces (%). Deviation of the measured Gaussian curvature (numerically calculated) of the QCGC surfaces from the Gaussian curvature of the undeformed sphere. The deviation is expressed as a percentage of the Gaussian curvature of the initial sphere.The different simulations correspond to $\mu = 1.5$ and $\lambda = 1$, 6 and 20. (Left) View from an angle. (Middle) View from the side. (Right) View from the top.

3 Preparation of the ping-pong ball for the experiments.

First the aperture was drawn on the pingpong balls. The aperture constituted of six arcs of a great circle (Fig. 3B of main text). The drawing was carefully done to ensure that the aperture was as symmetric as possible. The ping-pong balls were cut along the drawing using a Dremel rotary tool. Each ball was positioned between two glass slides so that its axis of symmetry was perpendicular to the slides.The parallelepiped constituted by the two glass blades containing the ping-pong ball was scanned successively on each of its eight faces. After the scanning, and the 3D reconstitution of the ping-pong ball, we symmetrized the surface by averaging the surface, its rotations of 120^o and of 240^o.

4 Simulations

Two types of mesh were used for the simulations: a regular triangular mesh and a randomized mesh. In the first case, each vertex of the regular mesh before the removal of the aperture had exactly six neighbors, except for the 12 special points that have only five neighbors. (Naturally after the removal of the aperture the boundary vertices at the rim of the aperture can have less than 5 bonds.) The lengths of each bond were to a very close approximation equal. The equations for the discretized stretching energy $E_{\rm str}$ and the discretized bending energy $E_{\rm bend}$ presented in the main text give a good approximation for the continuous in-plane stretching energy and the bending energy of the deformed shell. The bulk of the simulations was done for lattices with $N = 10242$ points (total number before the removal of the aperture), and a subset was repeated for $N = 40962$ points to verify that lattice size did not affect the quasi-inextensional shape.

The effect of the five-fold disinclinations in the original, regular tessellation of the shell was not expected to be big for the open, aperturate structures that we investigated, as the asymmetric nature of the load and geometry dominate over the influence of the lattice disclinations. Nevertheless, we verified our regular mesh computational results by repeating the simulations for a randomized mesh. The randomized mesh was produced by thermalizing the original regular mesh and performing a Delaunay triangulation to find the bonds of the new, randomized mesh. The new, randomized tessellation has multiple points with coordination 5 or 7, and these points were not regularly arranged. Although the discretized energy for the regular triangular lattice $E_{\rm str}$ is still valid for the randomized mesh, the discretized bending energy needed to be adapted. In this work, we found that the bending energy presented in (Gompper, 1996) worked well for our tessellation:

$$E_{\rm bend}(\{\vec{r}\}) = -\frac{1}{2}\kappa \sum_{<mk>} \nu_{mk} \cos(\phi_{mk} - \phi^0_{mk}) \tag{50}$$

where:

$$\nu_{mk} = 2/(\cot(\theta_1) + \cot(\theta_2)) \tag{51}$$

and θ_1, θ_2 are the two angles of the triangular facets opposite the link mk.

The parameter θ_0 that determines the $|\theta|$ range in the definition of the aperture is obtained by the solution of the following two equations:

$$(\cos(\frac{2\pi}{n}) - 1)(\cos(n\theta_0)^{m_s}\cos(\theta_0) - x_o) - \sin(\frac{2\pi}{n})(\cos(n\theta_0)^{m_s}\sin(\theta_0)) = 0 \tag{52}$$

$$\sin(\frac{2\pi}{n})(\cos(n\theta_0)^{m_s}\cos(\theta_0) - x_o) + (\cos(\frac{2\pi}{n}) + 1)(\cos(n\theta_0)^{m_s}\sin(\theta_0)) = 0 \tag{53}$$

5 Stretching and bending energy

Using formulas 7 and 8, appropriately adjusted for the case of a non-uniform mesh, we computed the bending and stretching energy for the different simulations at the different

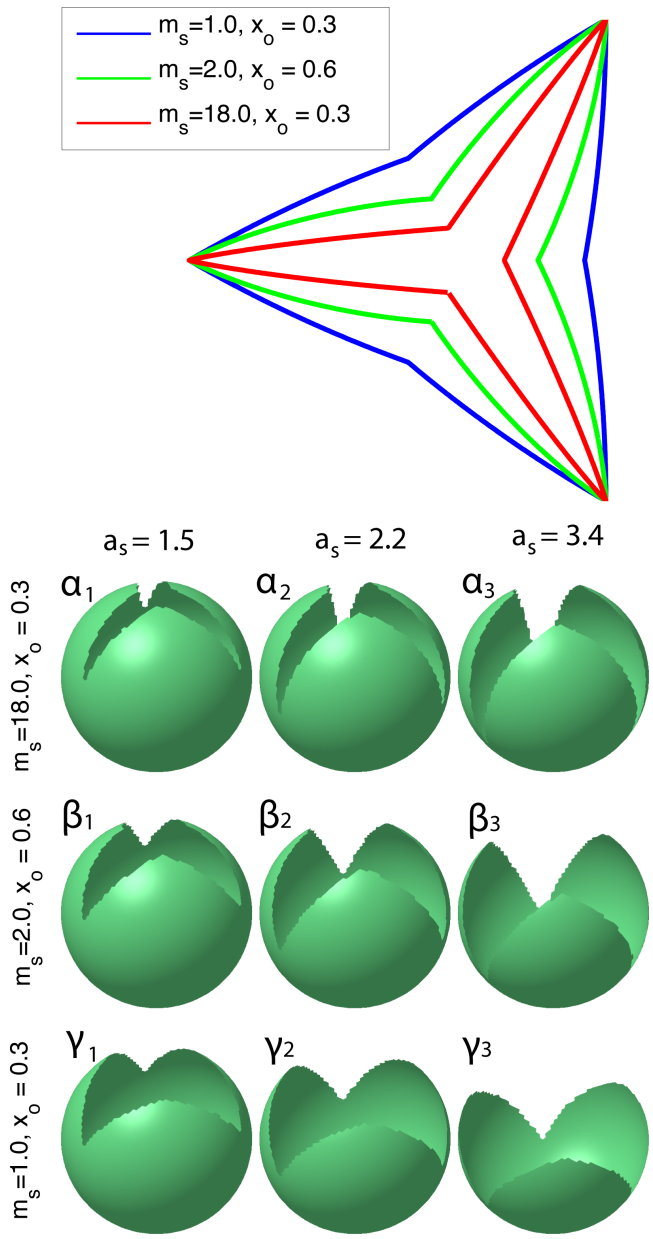

Figure 2: Design of the 9 shell of the simulations and corresponding parameters. The shells are identified in the text and the figure by the α_{1-3}, β_{1-3} and γ_{1-3}.

deformation stages. We observe that the bending energy is generally more than ten times bigger than the stretching energy (See Suppl. Fig. 3).

	ϕ		$E_{stretch}$				E_{bend}			
	ϕ_{min}	ϕ_{max}	**1**	**2**	**3**	**4**	**1**	**2**	**3**	**4**
α_1	0.96	1.40	0.30	0.50	0.60	ND	3.40	6.70	10.80	ND
α_2	0.77	1.40	0.60	0.80	0.80	0.90	7.20	13.60	17.70	23.00
α_3	0.56	1.33	0.80	1.20	1.30	1.30	12.10	24.10	32.00	39.40
β_1	0.96	1.25	0.90	1.80	2.60	ND	8.30	18.10	28.70	0.00
β_2	0.74	1.11	1.30	2.60	3.70	4.20	11.90	27.00	44.00	59.10
β_3	0.50	0.93	2.50	4.30	5.30	5.80	22.20	47.60	71.50	95.90
γ_1	0.96	1.36	0.60	1.10	1.40	ND	4.90	10.30	16.60	ND
γ_2	0.74	1.25	0.70	1.10	1.30	1.50	10.80	23.50	34.20	45.30
γ_3	0.50	1.11	1.20	2.10	2.50	2.30	16.70	36.50	57.10	80.60

Figure 3: Bending and stretching energy of the simulations.
The letters α_{1-3}, β_{1-3} and γ_{1-3} stand for the 9 simulated aperturate shells. The numbers from 1 to 4 stand for successive deformation stage of each shells. ϕ_{max}, ϕ_{min} correspond to the maximal and minimal geodesic coordinate of the shells for the top end and the corner respectively. The letters ND are used for big deformations, when the line in the symmetry plane did not lie closer than 2 % to any of the quasi CGC surfaces that we sampled in the first step of the derivation of best fit routine (See Suppl. Figure 5). The bending energy is generally more than ten times bigger than the stretching energy.

6 Quality of the fit

To project the experimental aperture of the ping-pong ball to the quasi-CGC surface, we successively project the aperture on the surface in the $x-y$ plane and $y-z$ plane and remove the area that is inside the projection. Similarly, for the simulation, we perform an orthogonal projection of the aperture to the surface and remove the points that fall inside the projected aperture margin.

To reduce the time to find the best fit for a given deformed shell, we proceed in two successive steps. Using the analytical formula for the line in the plane of symmetry (see ESI Sec. 1.2), we evaluate the surface along this line for a wide range of parameters (μ, λ). In order to efficiently search the parameter space (μ, λ), we first choose the parameters whose cross-section at the plane of symmetry lies closer than 2% of the spherical shell diameter to the deformed experimental or computationally obtained surface. The surface can be subdivided in sixth sectors (subunits) that are equal modulo a rotation and a mirror symmetry. The second step of the minimization was to calculate for each of the parameters of the reduced space the distance between the corresponding subunit and the target shell. We observed that independently of the exact shape of the boundary, the lower the corner of the shell, the higher the deformation that can be reached without stretching, and the longer is the validity of the fit (Fig. 4, 5).

7 Invariance of the corner angle

As the shell is thin and its deformation isometric, the angle at the three corners does not vary. This can be observed by superimposing the angle at the corner for the same shell at different degree of deformation (See Suppl. Fig. 6).

References

M. Berger, B. Gostiaux Gomtrie diffrentielle : varits, courbes et surfaces. *Presses universitaires de France* (1992) p47

G. Gompper and D. M. Kroll Random Surface Discretizations and the Renormalization of the Bending Rigidity *Journal de Physique I* (1996), 6, 1305–1320.

M. Spivak. Differential geometry, tome 5. *Publish or Perish Inc.* (1979)

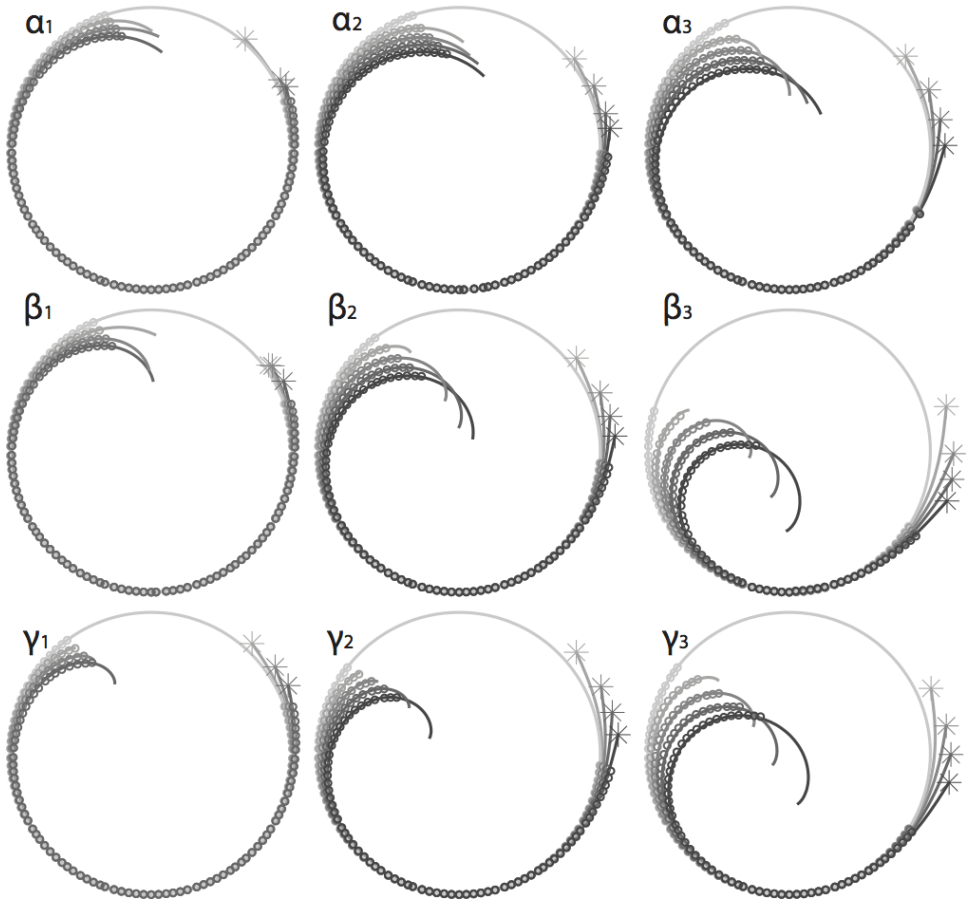

Figure 4: Fit of the lines situated in the symmetry planes of the shells. The letters α_{1-3}, β_{1-3} and γ_{1-3} stand for the 9 simulated aperturate shells of the Suppl. Fig. 2. The lower the corner is (e.g. α_3, β_3 and γ_3), the higher the deformation the shell can be correctly approximated by our family of solutions.

	ϕ		$\Delta h/h$				d_{max}				d_{mean}			
	ϕ_{min}	ϕ_{max}	**1**	**2**	**3**	**4**	**1**	**2**	**3**	**4**	**1**	**2**	**3**	**4**
α_1	0.96	1.40	0.02	0.05	0.08	ND	1.04	0.71	1.01	ND	0.20	0.14	0.18	ND
α_2	0.77	1.40	0.05	0.08	0.11	0.13	0.68	0.83	0.56	0.58	0.18	0.17	0.13	0.11
α_3	0.56	1.33	0.06	0.10	0.14	0.17	0.47	0.52	0.64	0.90	0.15	0.12	0.17	0.32
β_1	0.96	1.25	0.03	0.06	0.09	ND	0.45	0.34	0.69	ND	0.11	0.10	0.17	ND
β_2	0.74	1.11	0.03	0.06	0.09	0.13	0.61	0.30	0.27	0.37	0.16	0.12	0.08	0.11
β_3	0.50	0.93	0.03	0.06	0.12	0.19	0.99	0.51	0.61	0.74	0.26	0.12	0.21	0.30
γ_1	0.96	1.36	0.03	0.06	0.09	ND	0.65	0.48	0.52	ND	0.16	0.11	0.11	ND
γ_2	0.74	1.25	0.04	0.08	0.12	0.15	0.43	0.50	0.70	1.00	0.14	0.16	0.16	0.17
γ_3	0.50	1.11	0.05	0.11	0.17	0.21	1.10	1.13	1.30	1.31	0.30	0.34	0.37	0.34

Figure 5: Quality of the fit for the 9 simulations at different stages of deformation. The letters α_{1-3}, β_{1-3} and γ_{1-3} stand for the 9 simulated aperturate shells. The numbers from 1 to 4 stand for successive deformation stages of each shell. ϕ_{max}, ϕ_{min} correspond to the maximal and minimal geodesic coordinate of the shells for the top end and the corner respectively. $\frac{\Delta h}{h}$ stands for the extent of deformation (i.e $\frac{h_0-h}{h_0}$ where h_0 is initial height of the shell). d_{max} and d_{mean} correspond to the maximal and the mean distance between the deformed shell and its best fit among the quasi CGC surfaces. d_{max} and d_{mean} are given in % of the diameter. ND signifies that at higher deformation the line in the symmetry plane did not lie closer than 2% of any of the quasi CGC surfaces that we sampled in the first step of the minimization.

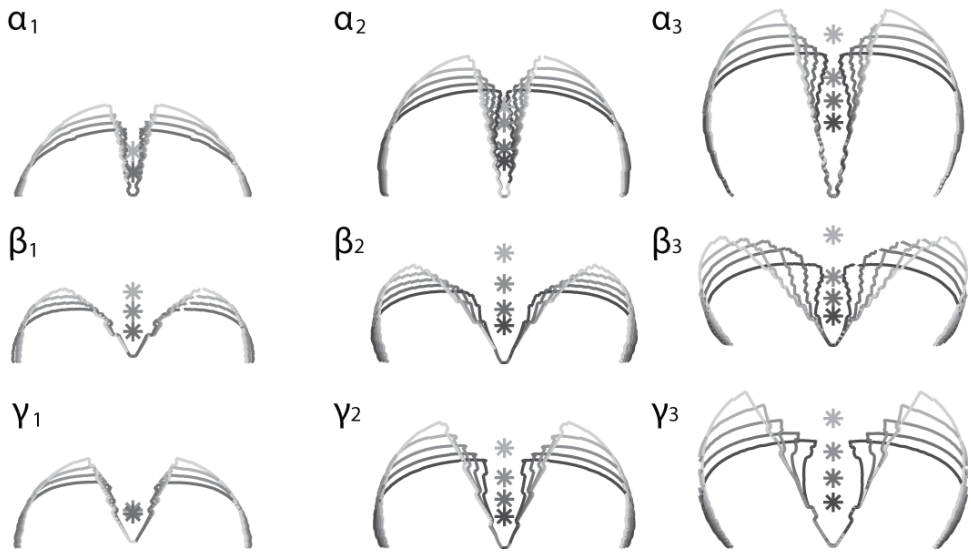

Figure 6: Invariance of the angle of the aperture contour and visualization of the singularity height. The letter corresponds to the one of the Suppl. Fig. 2. For each shell, one of the three angles of the aperture is superimposed at the successive deformation stage to show its invariance. The star corresponds to the singularity of the quasi CGC surface best fit surface.